Observation of Conductance Quantization in Oxide-Based Resistive Switching Memory

Xiaojian Zhu, Wenjing Su, Yiwei Liu, Benlin Hu, Liang Pan, Wei Lu, Jiandi Zhang, and Run-Wei Li**

The past half of a century has witnessed the extension of Moore's law which describes the doubling of transistor density in an integrated circuit every two years or so.[1] However, traditional charge based flash memories now face significant challenges as the transistor size decreases further into nano-regime.[2,3] As one of the most promising candidates for future non-volatile memories, resistive random access memory (RRAM) with a simple sandwiched structure exhibits attractive performance metrics including excellent scaling potential, low power consumption, high speed, and good endurance.[4,5] In many RRAMs, the main working mechanism is believed to be the formation or rupture of nanoscale conductive filaments embedded in an insulating matrix, thus offering promise of achieving ultra-high density storage due to its nature of nanoscale transport.[5,6] Conducting filaments have been suggested by some direct or indirect approaches including *in-situ* transmission electron microscope observations[7,8] and the detection of local enhanced conductivity.[9,10] On the other hand, as the filament is reduced to atomic scale size and essentially forms a one-dimensional conduction channel, then, it is natural to expect that quantum size effects, such as quantized conductance, may come into play.[11–13] Indeed, in solid state electrolyte, it has been demonstrated that storing data at atomic scale with discrete conductance changes in units of quantum conductance is experimentally feasible.[14] Here, we report the observation of conductance quantization in a number of oxide-based devices, which reveal the formation and rupture of nanoscale conducting filaments are responsible for the resistance switching process. The conductance quantization behaviors can be well modulated and in turn can lead to multi-level storage for ultrahigh density memory applications.

Two oxide resistive switching devices with different electrodes have been used in this study. The main oxide film is a thin layer of zinc oxide (ZnO, 80 nm) sandwiched either between a pair of niobium (Nb) and platinum (Pt) electrodes or between two metallic Indium tin oxide (ITO) electrodes. We describe first the results from Nb/ZnO/Pt device which is schematically shown in **Figure 1**a. The pristine state of the fresh devices was high resistive with a resistance of 10^8–10^9 Ω read at 0.1 V. A positive voltage of around 6 V was first applied to the Nb electrode with a compliance current (I_{cc}) of 100 μA to switch the device to a conductive state, which corresponds to the Forming process. The device can then be reliably switched between a low-resistive state (LRS) and a high-resistive state (HRS). The switching processes from the HRS to LRS and from the LRS to HRS correspond to the Set process and the Reset process, respectively. Typical resistive switching curves are shown in Figure 1b. The switch threshold voltages were–0.7 ± 0.3 V for Reset and 0.9 ± 0.5 V for Set processes, respectively.

Interestingly, during the Forming and the resistive switching processes, multiple current jumps were detected. A representative plot of the conductance changes is shown in Figure 1c in a voltage range from 0.75 to 1.60 V during the Set process. The electrical conductance G was calculated as $G = I/V$, where I is the current and V is the voltage. G was recorded in units of the quantum conductance $G_0 = 2e^2/h$, where e is electron charge and h is Planck's constant. Several abrupt conductance changes can be clearly observed, each followed by a stable conductance plateau. For instance, at 0.8 V, the conductance abruptly changed from 1 G_0 to 3 G_0, followed by a plateau at 4 G_0 after an initial increase. Similarly, at 1.3 V, the conductance was switched from 4 G_0 to 6 G_0 in two steps with a separation of 1 G_0 followed by a conductance platform until 1.45 V where another conductance jump occurred. With further increasing the bias voltage, similar switches were observed repeatedly. By analyzing about two hundred similar G-V curves during the Forming and Set processes, we found that most of the conductance changes occur at integer multiples values of G_0, suggesting that the quantized conductance in switching process can be attributed to discrete quantum channels[13] (Figure 1d). Similar G-V curves with step-like conductance versus voltage have also been observed in the Reset process (Figure S1 in Supporting Information).

Prof. R.-W. Li, X. Zhu, W. Su, Y. Liu, B. Hu, L. Pan
Key Laboratory of Magnetic Materials and Devices
Ningbo Institute of Material Technology
and Engineering (NIMTE)
Chinese Academy of Sciences (CAS)
Zhuangshi Road 519, Ningbo, Zhejiang 315201, PR China
E-mail: runweili@nimte.ac.cn

Prof. R.-W. Li, X. Zhu, W. Su, Y. Liu, B. Hu, L. Pan
Zhejiang Province Key Laboratory of Magnetic Materials
and Application Technology
Ningbo Institute of Material Technology and Engineering (NIMTE)
Chinese Academy of Sciences (CAS)
Zhejiang, Ningbo 315201, People's Republic of China
Prof. W. Lu
Department of Electrical Engineering and Computer Science
University of Michigan
Ann Arbor, Michigan 48109, USA
E-mail: wluee@eecs.umich.edu
Prof. J. Zhang
Department of Physics and Astronomy
Louisiana State University
Baton Rouge, LA 70803, USA

DOI: 10.1002/adma.201201506

© 2012 WILEY-VCH Verlag GmbH & Co. KGaA, Weinheim

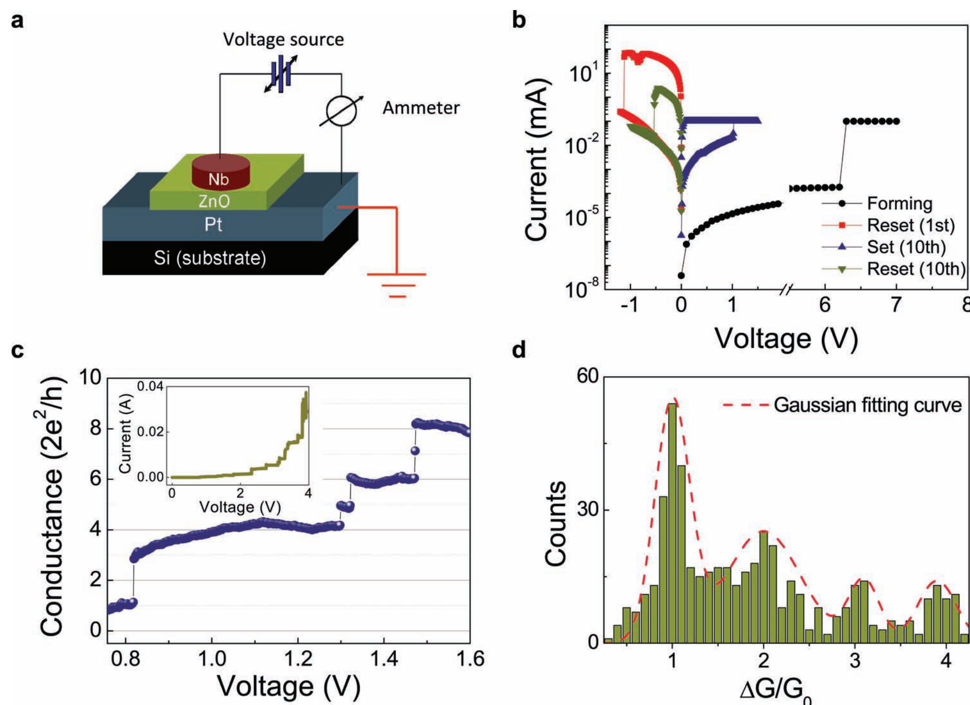

Figure 1. Resistance switching of Nb/ZnO/Pt devices. a) Schematic of a sandwiched Nb/ZnO/Pt structure. The Nb electrode is 100 μm in diameter. b) Typical bipolar resistive switching behaviors observed in the device. c) Measured conductance as a function of the bias voltage during the Set process. Inset: Corresponding *I–V* curve in a larger voltage range from 0 to 4 V. d) Histogram of the conductance changes $\triangle G$ obtained from the Forming and Set processes. Dotted line: Gaussian fitting curve of the histogram as a guide to the eye.

The existence of nanoscale filaments in Nb/ZnO/Pt structures, which gives rise to the quantized conductance behavior, was confirmed by conductive atomic force microscopy (C-AFM) imaging. The device structure for the C-AFM measurements also consists of a ZnO switching layer sandwiched between Pt and Nb electrodes, except here the fixed Pt electrode was replaced with a Pt AFM tip, as illustrated in **Figure 2**a. We found that at a low bias voltage < 1 V, no obvious change was detected in the C-AFM current map. After applying a bias voltage of 1 V, several bright spots with sizes of ~10 nm, corresponding to localized high conductive regions, emerge, as shown in Figure 2b. Further increasing the bias voltage results in more localized conductive spots and also increases in spot size. At 6 V, massive conductive spots appear in the current map (Figure 2c), indicating that the sample has been switched from the HRS to the LRS.[9,15] *I–V* measurements over these bright spots using the AFM tip as an electrode also show bipolar resistive switching behaviors similar to the lithographically-defined Nb/ZnO/Pt devices as illustrated in the inset of Figure 2c. These results clearly suggest that the nanoscale conducting filaments form in the switching medium. Importantly, we note that the size of the conductive filament (~10 nm) measured by C-AFM should only be considered as the upper size limit due to the limited C-AFM resolution. In addition, the C-AFM measures the size of the filaments at the surface, while the conductance of the filament will likely be dominated by a much narrower neck region beneath the surface, as have been reported in solid-electrolyte based RRAM devices.[5,16,17]

In order to verify the physical nature of the resistance switching behaviors in the Nb/ZnO/Pt structure, the resistance-temperature (*R-T*) relationship for the device after Forming process was measured. Here a device with a similar structure as the one in Figure 1a was used. The device in LRS state shows a typical temperature-dependence of a metallic conductor, in agreement with the picture of metallic filament conduction at LRS.[18,19] A sudden drop in resistance around 9.3 K was detected, which could be associated with the onset of superconductivity of Nb and suggests the filaments are composed of Nb. Based on the electrochemical filament formation theory,[5,20] Nb atoms can be oxidized to Nb ions during the Forming process under a positive bias voltage. These Nb ions will diffuse toward the Pt cathode through the ZnO film, and then become reduced into Nb atoms at the Pt cathode and eventually form the nanoscale conducting filaments. This hypothesis is consistent with the observations here. More discussions about the superconducting transition and Nb diffusion can be found in Supporting Information. The Reset process can be understood based on the electrochemical dissolution of Nb filaments with the assistance of Joule heating effect.[5] The atomic scale constraints in the filaments[11,13] in turn results in the observed quantum conductance behaviors.

The conductance quantization effects can be modified by controlling the current compliance during the Set or Forming processes. To avoid non-idealities when reading at high-field values and to observe stable quantized switching behaviors, the conductance was measured at 0.03 V in this study after

© 2012 WILEY-VCH Verlag GmbH & Co. KGaA, Weinheim

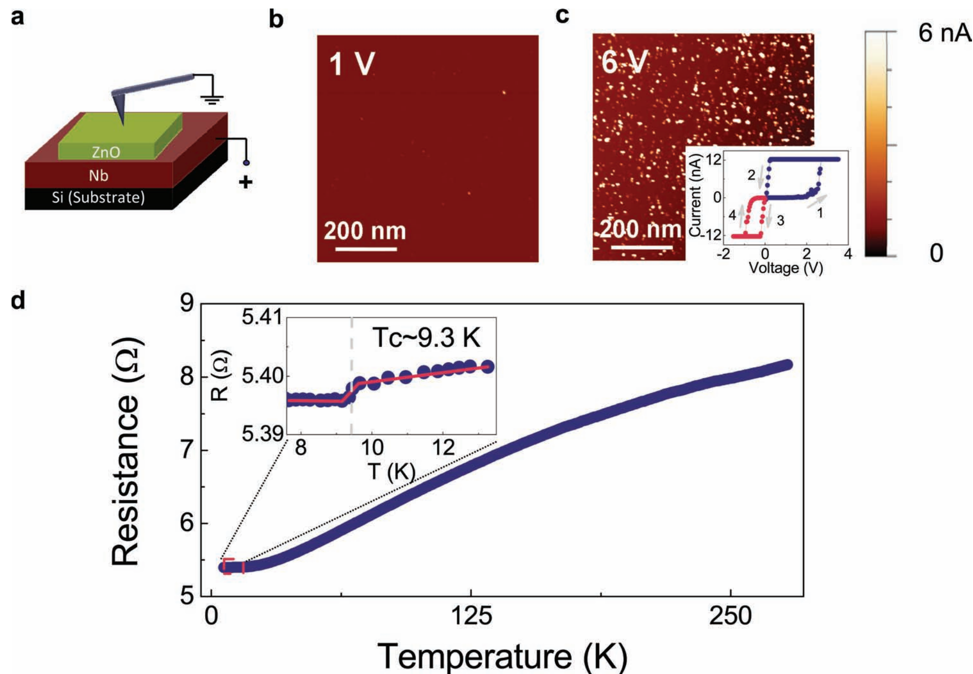

Figure 2. Observation of filamentary behaviors in a Nb/ZnO/Pt device using C-AFM. a) Schematic of the device structure and measurement setup. b,c) Current maps measured at biases of 1 V (b) and 6 V (c), respectively. Inset of (c): *I–V* characteristics over one bright spot measured by the AFM tip. d) Temperature dependence of the device resistance in LRS for a Cu (75 nm)/Nb (25 nm)/ZnO (80 nm)/Pt device. Inset: Zoomed-in curve showing a temperature range from 7.5 to 13.5 K.

each switching process with various Set voltages or current compliances. **Figure 3**a shows the *I–V* curves measured from the same Nb/ZnO/Pt device at different current compliance conditions. After a Set process with a compliance current of 100 μA, the device showed a stable conductance of 2.5 G_0 initially. As can be seen from Figure 3a, further increase in the current compliance during subsequent switching cycles correspondingly reduced the device resistance, as evident from the different slopes in the *I–V* curves in different sweeping processes. The conductance increased from 2.5 G_0 to 4.0 G_0 after the first voltage sweeping process with a compliance current of 2.5×10^{-4} A. Further increasing the current compliance leads to a monotonous increase of the conductance from 4.0 to 4.5, 6.5, and 8.5 G_0, respectively. In order to distinguish the quantum conductance behaviors from traditional multi-level storage behaviors, we performed controlled experiments in which the current compliance value was changed by small amounts each time and found that most of the conductance values tend to concentrate on the discrete quantum conductance values with remarkable margins between them (Figure S3 in Supporting Information), instead of distributed uniformly following the current compliance changes as expected for conventional multi-level storage.

Similar behavior was also observed in Reset process by controlling the Reset voltage range, as shown in Figure 3b. For instance, the initial conductance of the device was first switched to 14.5 G_0. After applying three negative bias voltages with increasing Reset voltage range, the conductance was sequentially reduced from 14.5 to 8, 4, and 1 G_0 (inset of Figure 3b). By applying a suitable current compliance during Set and a suitable voltage during Reset, the conductance can be switched between two stable states, here first 2 G_0 then 6 G_0, as shown in Figure 3c. The histogram of the conductance values obtained in the Set and Reset processes was plotted in Figure 3d. Most of the peaks concentrate around the integer multiples of 0.5 G_0, clearly demonstrating a quantized conductance behavior. The half integer quantum conductance values may originate from the adsorbed impurities on or in atom chains, which changes the constriction configuration and affects the electronic band structure, as have been discussed in the metal monatomic chains adsorbed with foreign impurities systems.[21–26]

Finally, we show that the quantized conductance phenomenon is intrinsic to the filamentary nature of the conducting channels in RRAM devices and can be observed regardless of the electrode material. To verify this, we fabricated ITO/ZnO/ITO sandwiched structures which show unipolar RS behaviors instead of bipolar switching as in the Nb/ZnO/Pt case. In oxide based unipolar switches it has been suggested that the resistive switching behaviors could originate from the formation/rupture of conducting filaments composed of defects, such as oxygen vacancies.[27] Nevertheless, similar to the Nb/ZnO/Pt devices, quantized conductance behaviors were also observed in ITO/ZnO/ITO devices (Figure S4 in Supporting Information), suggesting that this conductance quantization behavior is a universal feature in filamentary-based RRAM devices. Similar to the bipolar resistive switching characteristics in Nb/ZnO/Pt devices, the discrete quantum conductance values of the ITO/ZnO/ITO devices can be controlled during the Set process by controlling the current compliance from 4.0×10^{-3} to 9.0×10^{-3} A and during the Reset process by controlling the Reset

© 2012 WILEY-VCH Verlag GmbH & Co. KGaA, Weinheim

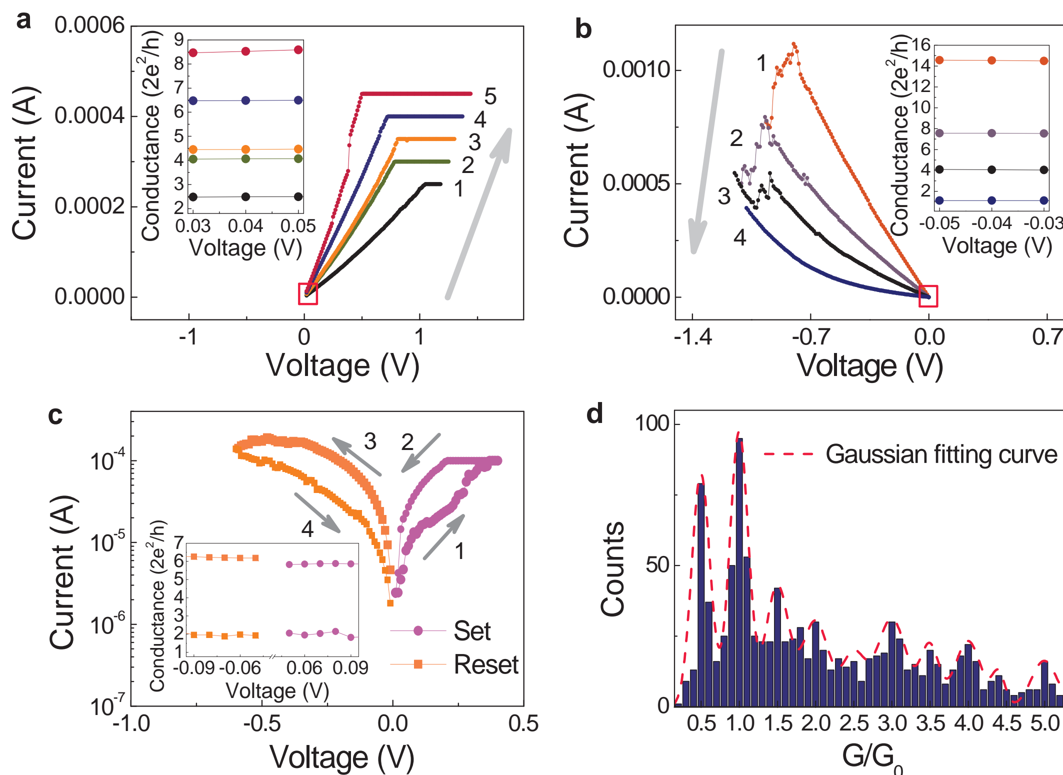

Figure 3. Quantized conductance behaviors in Nb/ZnO/Pt devices. a,b) Current-Voltage characteristics with various current compliances and voltage ranges in the Set (a) and Reset (b) processes, respectively. Inset: Corresponding conductance values read at 0.03, 0.04 and 0.05 V showing the conductance value is insensitive to the read voltage at low bias. c) Bipolar resistance switching behaviors between two discrete quantum conductance states. Inset: Corresponding conductance values read at low voltages. d) Histogram of the conductance values recorded at 0.03 V from a large number of Set and Reset processes. Dotted line: Gaussian fitting curve of the histogram as a guide to the eye.

voltage values from 2.0 to 4.2 V (**Figure** 4a–b). Reproducible switching between two states, here at 4.5 and 5.5 G_0, were also achieved by controlling these electrical parameters (Figure 4c). Statistics of the conductance values recorded at 0.03 V after each resistance switching process showed the conductance value concentrating at half integer quantum conductance as shown in Figure 4d, similar to that of the Nb/ZnO/Pt devices.

In addition, significant current oscillations were sometimes observed during the resistive switching process, as shown in Figure 4e (also see Figure S5 in Supporting Information). The current oscillations were reproducible in the same device and could also be observed in the backward voltage sweeping process (see Figure S6 in Supporting Information). The amplitudes of the conductance oscillations were found to also concentrate at integer values of G_0, indicating the oscillations are caused by the creation and rupture of nanoscale contacts inside the filaments (Figure 4f). Since unipolar resistive switching in the ITO/ZnO/ITO devices is caused by thermal effects, the conductance oscillations can be explained by the competition between the field-assisted formation and thermally-induced rupture of filaments at the right applied voltage and current range, as has been discussed in similar devices.[28–30]

In summary, we report quantized conductance behaviors in oxide-based sandwiched structures. The conductance quantization behaviors can be attributed to the creation and annihilation of atomic scale conducting filaments inside the insulating matrix. These studies clearly reveal the scaling potential of these two-terminal resistive switching devices, and can be used to achieve multi-level data storage. In addition, the controlled formation of atomic scale conduction channels in simple two-terminal devices in air and at room temperature can provide a platform to develop new one-dimensional nano-devices based on quantum effects. For example, by replacing the electrode material with magnetic metals or oxides and replacing the insulating layer with complex oxide such as multiferroic materials, one can potentially study strongly correlated effects in a confined channel that can be tuned by an applied electrical field.

Experimental Section

Sample preparation: 80-nm-thick ZnO films were deposited on a commercially available $Pt/Ti/SiO_2/Si$ substrate by magnetron sputtering a ZnO target in an atmosphere of argon and oxygen. The 100-nm-thick Nb top electrodes with a diameter of 100 μm were obtained by sputtering a Nb target in pure argon atmosphere using a magnetron sputter with a metal mask covered on the ZnO film. For the ITO/ZnO/ITO devices, the ZnO film was deposited on commercial Indium titanium oxide (ITO) glass under the same condition as that for Nb/ZnO/Pt structures. The 100-nm-thick ITO top electrodes were deposited by sputtering an ITO target using a pulsed laser deposition system.

© 2012 WILEY-VCH Verlag GmbH & Co. KGaA, Weinheim

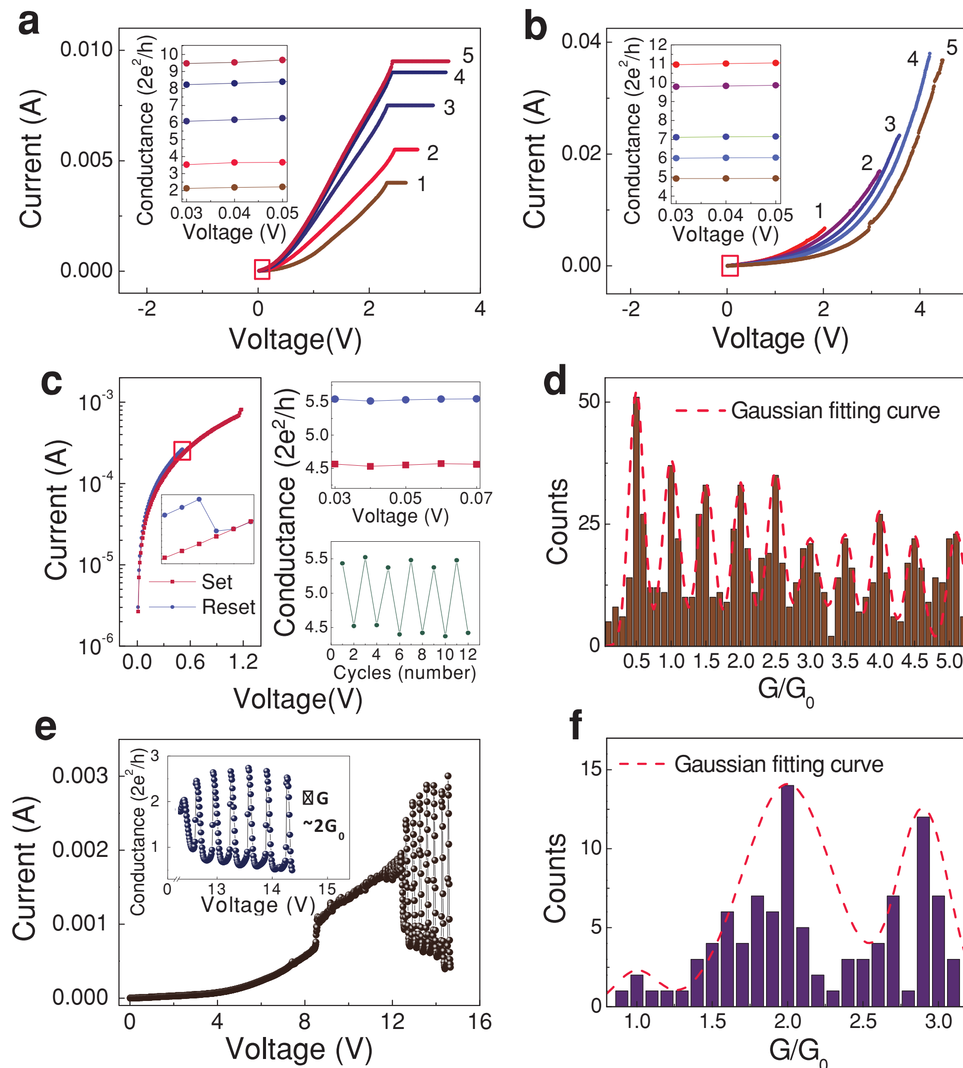

Figure 4. Quantized conductance behaviors in ITO/ZnO/ITO devices. a,b) *I*–*V* curves with various current compliances and voltage ranges in Set (a) and Reset (b) processes, respectively. Inset: Corresponding conductance values read at 0.03, 0.04 and 0.05 V in different sweeping cycles. c) Resistance switching between two quantum conductance states. Inset: zoom-out of the rectangular region. Right: conductance values read at 0.03, 0.04, 0.05, 0.06 and 0.07 V (upper panel) and the corresponding endurance test results between the conductance state of 4.5 and 5.5 G_0 (lower panel). d) Histogram of the recorded conductance values at 0.03 V from a number of Set and Reset processes. Dotted line: Gaussian fitting curve of the histogram as a guide to the eye. e) Current oscillations observed during the Set process. Inset: Corresponding *G*–*V* curve in a voltage range from 12.3 to 14.4 V. f) Histogram of the oscillation amplitude extracted from 14 curves similar to that in Figure.4e. Dotted line: Gaussian fitting curve of the histogram as a guide to the eye.

Measurements: The resistance switch behaviors of the devices were characterized at room temperature in air using a Keithley 4200 semiconductor parameter analyzer. An atomic force microscopy (Dimension V, Veeco) equipped with a conducting cantilever coated with Pt/Ir was employed for C-AFM measurements of the ZnO/Nb devices. During the measurement, the tip was always grounded while a bias voltage was applied on the Nb film.

Temperature dependences of the resistance for various devices at LRS were studied by physical property measurement system (PPMS, Quantum Design) using a conventional two-probe method. After Forming process with a current compliance of 100 μA, the devices were set to LRS. Afterwards, the devices were connected with thin platinum (Pt) wires with high conductive silver glue (EPO-TEK H20E produced by Epoxy Technology, Inc. volume resistivity @ 23° ≤ 0.0004 ohm-cm) followed by welding of the Pt wires to the PPMS sample stage. During the R-T measurement process, a constant-current mode with an excitation current of 50 μA was used.

Supporting Information

Supporting Information is available from the Wiley Online Library or from the author.

Acknowledgements

We thank Dr. F. Zhuge and Prof. J. Suñé for discussions. This work was supported by State Key Research Program of China (973 Program,

© 2012 WILEY-VCH Verlag GmbH & Co. KGaA, Weinheim

2009CB930803, 2012CB933004), National Natural Science Foundation of China, Zhejiang and Ningbo Natural Science Foundations, Chinese Academy of Sciences (CAS), and Science and Technology Innovative Research Team of Ningbo Municipality (2011B82004, 2009B21005).

Received: April 15, 2012
Published online: June 18, 2012

[1] M. Lundstrom, *Science* **2003**, *299*, 210.
[2] R. Waser (ed.), *Nanoelectronics and Information Technology*, Wiley-VCH, Weinheim **2003**.
[3] K. Kim, G.-H. Koh, *Proc. Int. Conf. Microelectronics*, Nis, Serbia **2004**, May.
[4] M.-J. Lee, C. B. Lee, D. Lee, S. R. Lee, M. Chang, J. H. Hui, Y.-B. Kim, C.-J. Kim, D. H. Seo, S. Seo, U.-I. Chung, I.-K. Yoo, K. Kim, *Nat. Mater.* **2011**, *10*, 625.
[5] R. Waser, R. Dittmann, G. Staikov, K. Szot, *Adv. Mater.* **2009**, *21*, 2632.
[6] K. Szot, W. Speier, G. Bihlmayer, R. Waser, *Nat. Mater.* **2006**, *5*, 312.
[7] S.-J. Choi, G.-S. Park, K.-H. Kim, S. Cho, W.-Y. Yang, X.-S. Li, J.-H. Moon, K.-J. Lee, K. Kim, *Adv. Mater.* **2011**, *23*, 3272.
[8] Z. Xu, Y. Bando, W. Wang, X. Bai, D. Golberg, *ACS Nano* **2010**, *4*, 2515.
[9] S. C. Chae, J. S. Lee, S. Kim, S. B. Lee, S. H. Chang, C. Liu, B. Kahng, H. Shin, D.-W. Kim, C. U. Jung, S. Seo, M.-J. Lee, T. W. Noh, *Adv. Mater.* **2008**, *20*, 1154.
[10] J. Y. Son, Y.-H. Shin, *Appl. Phys. Lett.* **2008**, *92*, 222106.
[11] K. Takayanagi, *JSAP International* **2001**, *3*, 3.
[12] C. J. Muller, M. A. Reed, *Science* **1996**, *272*, 1901.
[13] H. Ohnishi, Y. Kondo, K. Takayanagi, *Nature* **1998**, *395*, 780.
[14] K. Terabe, T. Hasegawa, T. Nakayama, M. Aono, *Nature* **2005**, *433*, 47.
[15] R. Muenstermann, T. Menke, R. Dittmann, R. Waser, *Adv. Mater.* **2010**, *22*, 4819.
[16] R. Waser, *Microelectron. Eng.* **2009**, *86*, 1925.
[17] C. Schindler, G. Staikov, R. Waser, *Appl. Phys. Lett.* **2009**, *94*, 072109.
[18] Y. C. Yang, F. Pan, Q. Liu, M. Liu, F. Zeng, *Nano Lett*. **2009**, *9*, 1636.
[19] Q. Liu, S. Long, H. Lv, W. Wang, J. Niu, Z. Huo, J. Chen, M. Liu, *ACS Nano* **2010**, *4*, 6162.
[20] T. Tsuruoka, K. Terabe, T. Hasegawa, M. Aono, *Nanotechology* **2010**, *21*, 425205.
[21] C. Untiedt, D. M. T. Dekker, D. Djukic, J. M. van Ruitenbeek, *Phys. Rev. B* **2004**, *69*, 081401.
[22] C. Z. Li, H. X. He, A. Bogozi, J. S. Bunch, N. J. Tao, *Appl. Phys. Lett.* **2000**, *76*, 1333.
[23] M. Kiguchi, T. Konishi, K. Murakoshi, *Phys. Rev. B* **2006**, *73*, 125406.
[24] Sz. Csonka, A. Halbritter, G. Mihaly, E. Jurdik, O. I. Shklyarevskii, S. Speller, H. V. Kempen, *Phys. Rev. Lett.* **2003**, *90*, 116803.
[25] C. Shu, C. Z. Li, H. X. He, A. Bogozi, J. S. Bunch, N. J. Tao, Phys. *Rev. Lett.* **2000**, *84*, 5198.
[26] W. A. de Herr, S. Frank, D. Ugarte, *Z. Phys. B* **1997**, *104*, 469.
[27] J. W. Seo, J.-W. Park, K. S. Lim, J.-H. Yang, S. J. Kang, *Appl. Phys. Lett.* **2008**, *93*, 223505.
[28] D.-K. Kim, D.-S. Suh, J. Park, *IEEE Electron Dev. Lett.* **2010**, *31*, 600.
[29] M. D. Pickett, J. Borghetti, J. J. Yang, G. Medeiros-Ribeiro, R. S. Williams, *Adv. Mater.* **2011**, *23*, 1730.
[30] Y. Li, S. Long, H. Lv, Q. Liu, W. Wang, Q. Wang, Z. Huo, Y. Wang, S. Zhang, S. Liu, M. Liu, *IEEE Electron Dev. Lett.* **2011**, *32*, 363.

© 2012 WILEY-VCH Verlag GmbH & Co. KGaA, Weinheim